Research Article

Mohamed S. Hodhod[#], Abdel-Rhman Z. Gaafar*[#], Bandar M. AlMunqedhi, Abdalla Elzein, Abdelmalik M. Abdelmalik

Exploitation of mangliculous marine fungi, *Amarenographium solium*, for the green synthesis of silver nanoparticles and their activity against multiple drug-resistant bacteria

https://doi.org/10.1515/chem-2023-0184
received September 19, 2023; accepted December 2, 2023

Abstract: The green synthesis pathway for silver nanoparticles (AgNPs) used in bacterial treatment is regarded as crucial because of its cost-effectiveness, nontoxicity, and eco-friendliness. During the present work, the mangliculous marine fungi *Amarenographium solium* isolated from the Arabian Gulf Coast of Saudi Arabia were utilized for the synthesis of AgNP, through the bio-reduction of aqueous silver nitrate ($AgNO_3$) solution. The success in AgNP synthesis was visually identified by the development of dark brown color in the cell-free filtrate and was further confirmed by ultraviolet–visible spectroscopy, which showed a peak at 425 nm. The AgNPs produced were further characterized using X-ray diffraction data analysis that proved the bioreduction of silver to 20 nm, and transmission electron microscopy revealed the formation of well-dispersed spherical nanoparticles with an average mean size of 12 nm. The optimization reaction parameters of temperature, pH, and metal salt concentration were carried out and resulted in a combination of 30°C, 7 and 1.5 mM, respectively, for rapid and maximum yield production. The antibacterial activity of the produced nanoparticles was evaluated using the two-fold microdilution method and showed a minimum inhibitory concentration of 9.375 µg/mL of AgNP against multiple drug-resistant bacterial strains.

Keywords: marine fungi, silver nanoparticles, biosynthesis, characterization, optimization, antibacterial activity

1 Introduction

Multiple drug resistance is a global threat, driven by the extensive use of antimicrobials that results in the emergence of many different bacterial species with increased resistance frequencies, especially in developing countries due to poor sanitary conditions, the availability of antimicrobials without prescriptions, and low healthcare budgets that resulted in the limitation of access to new effective antibiotics [1]. World health leaders have named antibiotic-resistant microorganisms 'nightmare bacteria' that 'pose a catastrophic threat' as new forms of drug resistance can easily spread between continents and across international boundaries, causing infections with significantly high rates of morbidities and mortality [2,3].

Metal nanoparticles (m-NPs) have been shown to be effective antibacterial agents capable of bypassing resistance mechanisms and hindering their future resistance potential [4]. Many routes have been developed for the synthesis of m-NPs, including physical and chemical pathways, but concerns have been raised over the environmental pollution of these production routes, which generate massive

Both Mohamed S. Hodhod, Abdel-Rhman Z. Gaafar are considered as first co-authors.

* **Corresponding author: Abdel-Rhman Z. Gaafar,** Department of Botany and Microbiology, College of Science, King Saud University (KSU), P.O. Box 11451, Riyadh, Saudi Arabia, e-mail: agaafar@ksu.edu.sa, tel: +966-540329167
Mohamed S. Hodhod: Faculty of Biotechnology, October University for Modern Sciences & Arts, 6th October City, 12566, Egypt, e-mail: mshodhod@msa.edu.eg
Bandar M. AlMunqedhi: Department of Botany and Microbiology, College of Science, King Saud University (KSU), P.O. Box 11451, Riyadh, Saudi Arabia, e-mail: balmunqedhi@ksu.edu.sa
Abdalla Elzein: Institute of Integrative Nature Conservation Research (INF), Department of Integrative Biology and Biodiversity Research (DIBB), University of Natural Resources and Life Sciences (BOKU), Vienna, Austria, e-mail: abdalla.elzein@boku.ac.at
Abdelmalik M. Abdelmalik: Department of Plant Production, College of Food and Agriculture Sciences, King Saud University, Riyadh, Saudi Arabia, e-mail: aadam1@ksu.edu.sa
ORCID: Abdel-Rhman Z. Gaafar 0000-0001-6218-9572

amounts of toxic hazard byproducts. Nanobiotechnology has emerged due to the integration between biotechnology and nanotechnology providing a new route of synthesis for antibiotic production using "green chemistry," which is a clean, nontoxic, and environmentally friendly method used for the synthesis of m-NP by exploiting biological systems, i.e., plants, algae, fungi, and bacteria [5–7].

Fungi are the most efficient biological system for nanoparticle synthesis due to several advantageous characteristics including extreme metal bioaccumulation abilities, elevated levels of tolerance, and their ability to secrete efficient nanoparticle bioreduction extracellular enzymes, which ease the nanoparticles synthesis scaleup, making the entire process more cost-effective [8,9]. Silver is widely used in nanoparticle synthesis over other metals, due to its powerful antibacterial effect [10].

However, the AgNPs produced have a wide variation in antibacterial potential depending on the bioreduction machinery possessed by different fungal species. Studies using fungi in silver nanoparticles (AgNPs) included the use of *Pleurotus ostreatus*, *Fusarium oxysporum*, and filamentous fungi, which have shown antibacterial activity against various pathogenic bacterial strains [11]. Green AgNPs have been identified as potential antibacterial agents against a variety of Gram-positive and Gram-negative pathogenic bacteria, including *Bacillus subtilis*, *Escherichia coli*, *Enterobacter aerogenes*, *Pseudomonas aeruginosa*, *Salmonella epidermidis*, *Salmonella typhimurium*, *Staphylococcus aureus*, *Streptococcus pneumoniae*, *Streptococcus pyogens*, and *Vibrio parahaemolyticus* [12–16].

Therefore, the continuous search for new fungal resources can yield new particles with different characteristics. Among these untapped resources are manglicolous fungi, which are the second largest ecological group that inhabits salt-tolerant shrubs, ferns, and palms that colonize intertidal zones of mudflats and banks of tropical and subtropical rivers and coastlines in many parts of the world [17,18]. This study aims to utilize the manglicolous fungi *Amarenographium solium* for the first time in the synthesis of AgNP and to evaluate their activity against multiple drug-resistant bacteria.

2 Materials and methods

2.1 Fungal isolation and growth conditions

Intertidal deteriorated wood samples originated from a mangrove stand on Tarout island in Saudi Arabia's Arabian Gulf Sea, at coordinates (26°35′43N to 50°3′51E). The morphological features of fruiting structures (conidiophores, conidiogensis, conidiomata, and conidia for anamorphic fungus) were used to identify *A. solium* [19]. The conidia were placed in seawater and photographed, measured, and described employing a compound microscope (China, Motic ACCU-scope 3002). A scanning electron microscope (SEM) (JOEL, JSM-6380 LA, Tokyo, Japan) was used to analyze *A. solium* further. To obtain single spore cultures of *A. solium*, we prepared *a* conidia suspension in seawater on a microscopic slide under sterilized condition. Small drops of suspension were placed on Petri plates containing glucose yeast agar GYA (10 g glucose, 1 g yeast extract, 18 g agar in 1 L of seawater) and incubated at 25°C in the dark. Petri plates were checked after 12 h for germinated conidia, which were then transferred to new GYA petri plates using sterile forceps and cultured in the dark at 25°C for 1–2 weeks [20]. A pure fresh culture of *A. solium* was maintained in glycerol solution (10%) at −80°C and registered in the Myco-Bank Molecular Microbiology Laboratory, Department of Botany and Microbiology, College of Sciences, King Saud University, under the ID number MF412.

2.2 Molecular identification of *A. solium*

Pure isolates were grown in yeast, maltose, and glucose broth (YMG) (4 g yeast extract, 10 g of glucose, 10 g malt extract in 1 liter of seawater) until sufficient mycelium was formed. Mycelium was harvested by centrifugation at 1,400 rpm for 10 min, then washed three times with sterile normal saline solution (0.89% NaCl). The DNA extraction procedure was carried out using the DNA extraction kit (QIAGEN; DNeasy Plant, Cell/tissue and Fungi DNA extraction kit, Venlo, The Netherlands) according to the manufacturer's instructions. The large ribosomal subunit (LSU rDNA) was amplified using the forward primer LROR and LR7 as reverse [21], while the small ribosomal subunit (SSU rDNA) was amplified using NS1 as forward and NS8 as reverse [22] (Table 1).

Sequencing was carried out by Macrogen Inc. (Korea) using MGTMTaq-HF DNA Polymerase; with cycling profile: initial denaturation at 96°C for 3 min, followed by 45 cycles of 96°C for 15 s, 52°C for 45 s, 72°C for 1 min 30 s of denaturation, annealing and extension respectively, then a final extension at 72°C for 7 min. After that, sequences were edited using

Table 1: Forward and reverse primers along with their sequences

Primer	Sequence (5′–3′)
LR0R	ACCCGC TGA ACT TAA GC
LR7	TACTAC CAC CAA GAT CT
NS1	GTAGTCATATGCTTGTCTC
NS8	TCCGCAGGTTCACCTACGGA

Sequencher, Demo V4.10.1 for sequence enhancement, aligned with their relatives from GenBank within Clustal X [23] and then manually adjusted. Sequences were then uploaded to GenBank via BanKit and the accession numbers to the sequences were given as (MK007121) and (MK007122) for the large and small ribosomal subunits, respectively. Phylogenetic analysis was performed using the Molecular Evolutionary Genetics Analysis program (MEGA X) (Kumar et al. [24]) to generate maximum likelihood (ML) trees and maximum parsimony (MP) trees [25,26].

2.3 Biosynthesis of AgNPs

A. solium was propagated in 250 Erlenmeyer flasks with 100 mL of YMG sea-water medium. For 5 days at 25°C, cultured flasks were allowed to incubate in a rotating shaker at 200 rpm. Extracellular biosynthesis of AgNP was carried out using the supernatant (potential bioreduction agent) obtained after centrifugation of the cultured flasks at 1,400 rpm for 10 min and the metal salt precursor solution 1 mM silver nitrate ($AgNO_3$) (HPLC grade – Sigma-Aldrich). The supernatant was added to the $AgNO_3$ solution in a 1:9 ratio. The metal salt's bioreduction was immediately identified by the development of a brown hue, and it was then placed on a rotating shaker (200 rpm) at 25°C for 72 h to finish the reduction process [27].

2.4 Optimization of the AgNP reaction for rapid synthesis

Yield optimization was performed using a factorial experiment in a completely randomized design CRD [28]. The experiment was carried out using temperature, metal salt concentration (mM), and pH as the main factors, each with three levels and three replicates. AgNP yield (mg/mL) was the response variable and was determined using ultraviolet–visible spectroscopy (UV-1800 Shimadzu Spectrophotometer; Japan). Biosynthesis was estimated using the standard curve for the synthesized metal and the linear equation $Y = XS \pm I$ "where Y = yield (mg/mL), S = slope, and I = intercept" [29].

2.5 Characterization of AgNPs

2.5.1 X-ray diffraction (XRD)

The mean size of AgNPs was determined by XRD-Ultima IV Rigaku; USA on the corresponding drop-coated film of nanoparticle solution. The Scherer formula $d = 0.9\ \lambda/\beta \cos\theta$ was employed to calculate the mean size of the generated nanoparticles, where d is the mean diameter of the nanoparticles, λ is the wavelength of the X-ray radiation source, β is the complete angular width around half maximum at the diffraction angle of the XRD peak, and θ is the angle of Bragg [30].

2.5.2 Transmission electron microscopy (TEM)

The physical characteristics of the produced AgNPs, involving their form and size, were studied and characterized employing a TEM apparatus (JEOL-JEM-1011; Tokyo, Japan). The sample was generated by drop-coating a sheet of AgNPs (100%) over carbon-coated copper TEM grids. Prior to measuring, the films on the TEM grids were dried.

2.5.3 Fourier transform infrared (FTIR) spectroscopy

FTIR spectroscopy (PerkinElmer 1000 FT-IR, USA) was used to identify candidate biomolecules involved in AgNP bioreduction. The biosynthesized nanoparticles were centrifuged at 14,000 rpm for 15 minutes before being re-dispersed in sterile distilled water to eliminate any uncoordinated biological molecules. The process of centrifugation and redispersion in sterile distilled water was carried out three times to guarantee greater separation of free entities from m-NP. The purified pellets were subsequently dried, and the powders were analyzed using FTIR spectroscopy.

2.6 Antibacterial activity

The antibacterial ability of the m-NP produced was tested against eight pathogenic bacterial species (Table 2) obtained from the Microbiology Laboratory, Department of Botany and Microbiology, College of Science, King Saud University. A two-fold microdilution method was used to determine the minimum inhibitory concentration MIC using a 96-well plate (FALCON, France); 1,200 µg/mL was the starting concentration for AgNP, while 9.375 µg/mL was the end point concentration reached by serial microdilutions. Plates (three replicates) were then measured using an ELISA reader (ELX 800 microplate reader; BioTek, USA). After MIC determination, aliquots of 50 µL from all wells that did not show bacterial growth were subcultured on Mueller-Hinton agar plates and incubated at 37°C for 24 h, to determine the minimum end point of bactericidal concentration.

Table 2: bacterial stains used to assess the potential of biosynthesized AgNP activity

	Bacterial strain	Type	Sensitivity
1	*E. coli*	Gram negative	Sensitive
2	*E. coli*		Resistant
3	*Acinetobacter baumannii*		Sensitive
4	*Acinetobacter baumannii*		Resistant
5	*S. aureus*	Gram-positive	Sensitive
6	*S. aureus*		Resistant
7	*S. epidermidis*		Sensitive
8	*S. epidermidis*		Resistant

2.7 Statistical analysis

A one-way analysis of variance was performed to analyze antibacterial activity data using IBM SPSS Statistics 25.

3 Results

3.1 Morphological identification

Using dissecting, compound and electron microscope, *A. solium* was recognized by its characteristics, including (1) Pycnidia 330–380 µm high, 210–245 µm in diameter, subglobose, immersed, brown to black, ostiolate, with circular opening, mature pycnidia that form a black mass of conidia on the surface of wood, (2) Conidia 37.5–46 × 13–18 µm, muriform, with (3-) 5 (-7) transverse septa and (0-) 1 (-2) longitudinal septa, clavate, with rounded apex and acute or truncate basal end acute or truncate, at first yellowish to olivaceous-brown, becoming brown at maturity, constricted at the central septum and slightly at the other septa, smooth with a gelatinous, striated, regular cap and sheath; the sheath is multilayered in young conidia, swelling and forming fibrillary material in water and eventually dissolving (Figure 1).

3.2 Phylogenetic analysis

3.2.1 Small subunit data set

A. solium proved to be a member of the Pleosporales Incertae-sedis family and formed a sister taxon to *A. solium* Abdel-Wahab, Hodhod, Bahkali, and K.D. Hyde. Forming a well-supported clade in the SSU data set (100/100 for ML/MP, respectively). The collected dataset included the query sequence and 20 taxa of which one belongs to the same order Pleosporales Incertae-sedis and includes three taxa from the closest families Massariaceae and Montagnulaceae. Two taxa of the order Dothideales were used as outgroup taxa. The small subunit dataset consisted of 1,828 total characters. The three most parsimonious trees were produced using a heuristic search; all produced trees with a tree length of 347 steps, a consistency index of 0.650943, a retention index of (0.753333), and the composite index is 0.592680 (0.490377) for all sites and parsimony-informative sites. The ML analysis produced one tree (–ln likelihood = 4603.62). ML and MP analyses produced trees with similar topologies (Figure 2).

3.2.2 Large subunit data set

A. solium proved to be a member of the Pleosporales Incertae-sedis family and formed a sister taxon to *A. solium* Abdel-Wahab, Hodhod, Bahkali, and K.D. Hyde. Forming a well- supported clade in the LSU data set (100/100 for ML/MP, respectively). The collected data set included the query sequence 37 taxa of which one belonging to the same order Pleosporales Incertae-sedis includes eight taxa from the closest family Trematosphaeriaceae. Two taxa from the order Dothideales were used as outgroup taxa. The large subunit data set consisted of 1,488 total characters. The three most parsimonious trees were produced using a heuristic search, all trees produced with a tree length of 1,129 steps, a consistency index of 0.482197, a retention index of (0.692447), and the composite index is 0.380263 (0.333896) for all sites and parsimony-informative sites. Maximum likelihood analysis produced one tree (–ln likelihood = 8444.79). The ML and MP analyzes produced trees with similar topologies (Figure 3).

3.2.3 Biosynthesis of AgNPs

Initial observation revealed the development of a dark brown color in the solution, indicating the bioreduction of the metal salt into AgNPs using the cell-free filtrate (CFF) of *A. solium*. Further confirmation of AgNP biosynthesis using ultraviolet–visible (UV–vis) spectroscopy with optical density ranging from 300 to 800 nm showed a large peak at 425 nm (Figure 4).

3.3 Factors affecting AgNP biosynthesis and optimization of its production

3.3.1 Effect of temperature

The silver (Ag) metal nanoparticle yield rate was directly affected by the change in temperature. $AgNO_3$ was

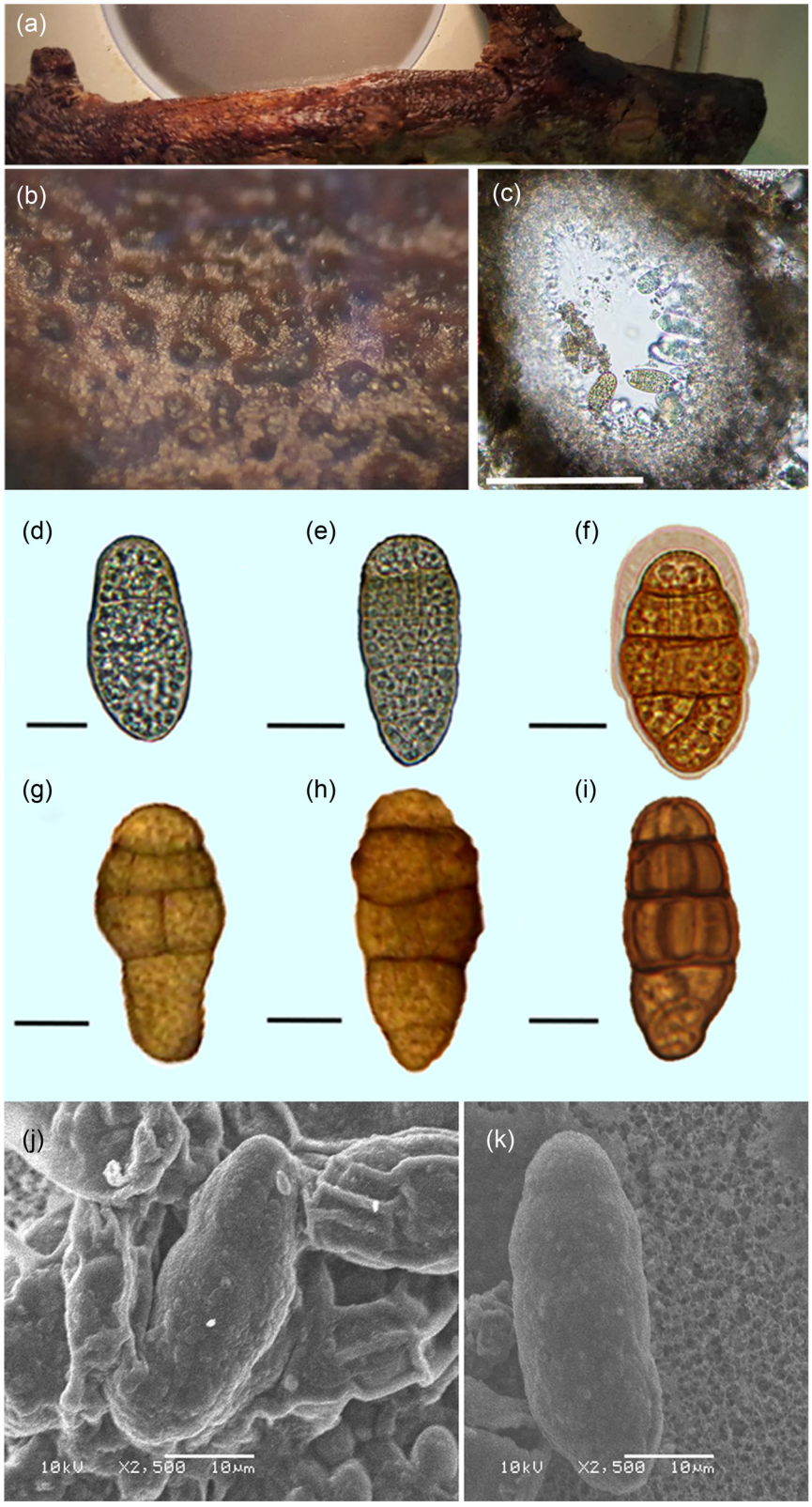

Figure 1: (a–e) *A. solium*. (a and b) Dissecting micrographs of the distribution of Pycnidia in a mangrove wood sample at different magnification. (c–i) Bright field light micrographs (from the holotype, mounted in water). (c) Longitudinal section of pycnidium bars: *C* = 50 µm. (d–i) Conidia at different developmental stages, taking various shapes. Bars: d–i = 5 µm. (j–k) SEM. (j) Rough-walled conidia. (k) Magnified conidia. Bars: a–e = 10 µm.

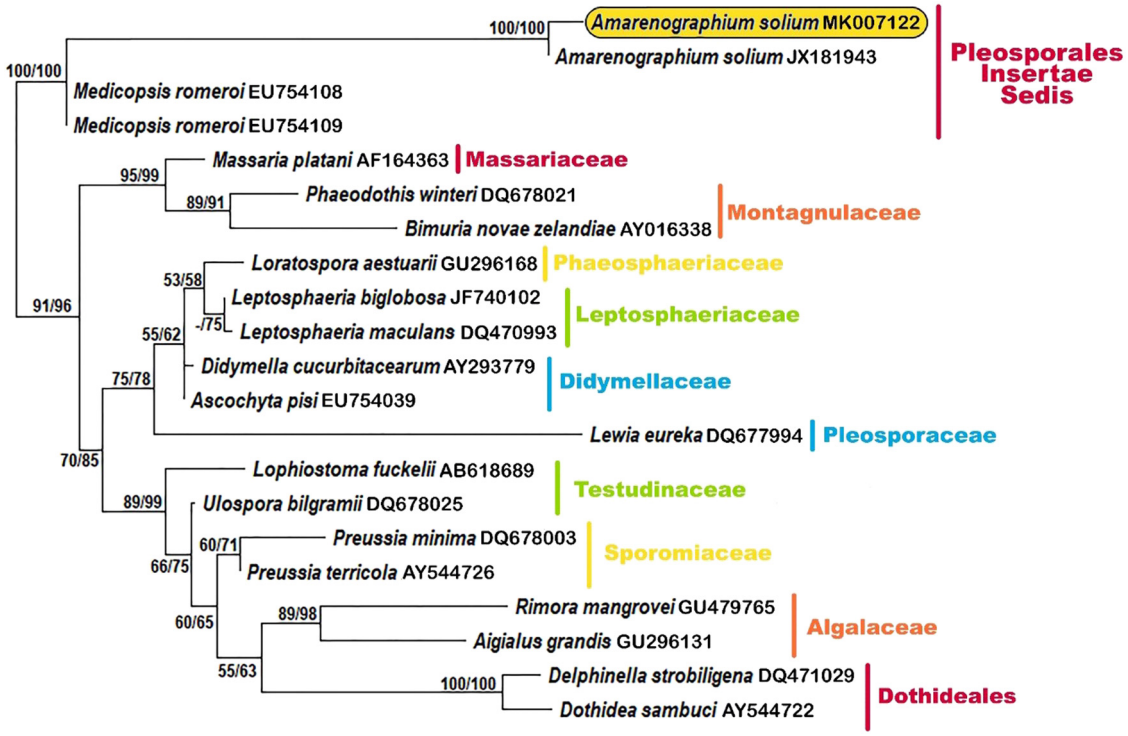

Figure 2: Phylogenetic tree of *A. solium* and related taxa, based on the nucleotide sequences of the small subunit sequence (SSU) gene. Numbers are bootstrap support for ML and MP, respectively. The fungus, *A. solium*, is highlighted.

incubated at different temperatures (20, 30, and 40°C). The metal nanoparticle yield showed a dramatic decrease when subjected to a low temperature of 20°C, while it showed the highest rates at 30°C. For a high temperature of 40°C, the result yield was slightly decreased compared to middle temperature trials.

3.3.2 Effect of metal salt concentration (mM)

The optimization experiment was designed to subject *A. solium* to different concentrations of metal salt ($AgNO_3$); concentrations applied were (0.5, 1, 1.5, and 2 mM). The fungi showed an increase in the yield rates until 1.5 mM, while 2 mM did not show any significant change in the bioreduction rate, the biosynthesized nanoparticles for silver were monitored using UV–vis spectral analysis, which provided evidence that the concentration of an increase in the metal salts is directly proportional to the result yield.

3.3.3 Effect of pH

A. solium sowed different responses along the pH gradient (3, 7, and 9), as biosynthesis levels showed their lowest levels at pH 3, while they showed their highest production levels at pH 7, yield at pH 9 showed a slight decrease in metal reduction compared to the pH 7 results.

3.3.4 Optimization of AgNPs

The optimum conditions (i.e., temperature, metal salt concentration [mM], and pH) for maximizing the yield (mg/mL) of biosynthesized nanoparticles were investigated from 27 experiments designed from all expected possibilities (Table 3). *A. solium* CFF showed a significant increase in yield (118.6 µg/mL) using the productive conditions in experiment 15 (pH = 7, temperature = 30°C and metal salt concentration = (mM) = 1.5); while the minimum yield (115.5 µg/mL) was recorded in experiment 7 (pH = 3, temperature = 40°C and metal salt concentration [mM] = 0.5) (Figure 5).

3.4 Characterization of AgNPs

3.4.1 XRD

The XRD of AgNPs corresponded to the characteristic face-centered cubic (FCC) silver lines indexed as (2.832), (1.987),

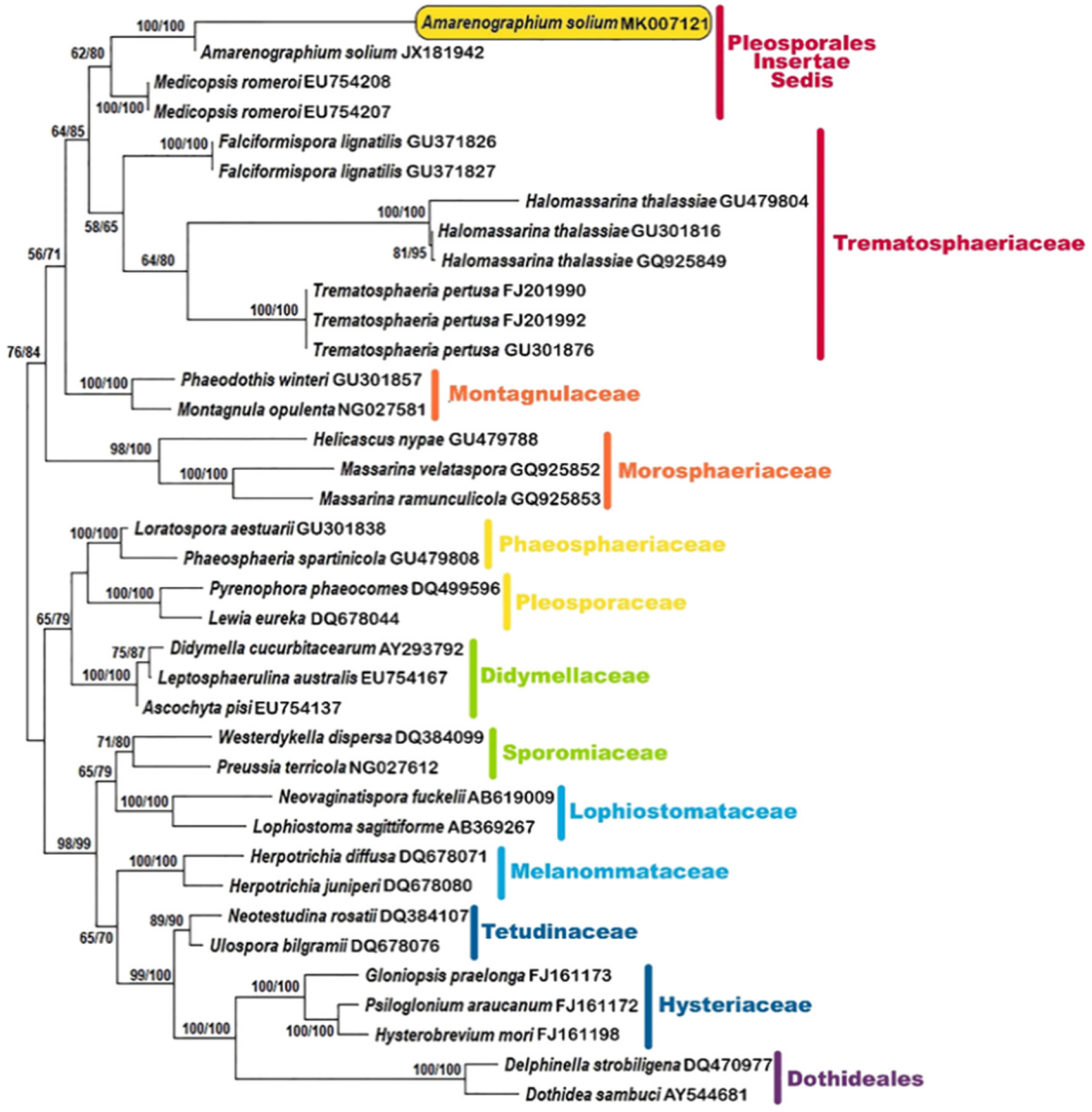

Figure 3: Phylogenetic tree of *A. solium* and related taxa, based on the nucleotide sequences of the large subunit sequence (LSU) gene. Numbers are bootstrap support for ML and MP, respectively. The fungus, *A. solium*, is highlighted.

(1.280), and (1.248) that were observed in these samples at diffraction angles of 32.6°, 46.1°, 74.7°, and 77.6°, respectively (Figure 6). The Scherer equation in the XRD data calculated the mean size of the AgNPs to be 20 nm.

3.4.2 TEM

The results of the synthesized m-NP revealed their surface characteristics and morphology based on shape and size. AgNPs under optimized conditions appeared to be spherical in shape with an average mean size of 12 nm (Figure 7).

3.4.3 FTIR spectroscopy

FTIR spectroscopy on AgNP showed absorbance at frequencies of 3,431, 2,919, 2,854, 1,624, 1,539, and 1,399 cm^{-1} (Figure 8).

3.4.4 Antibacterial activity

High antibacterial activity was shown against all Gram-positive and -negative bacteria, including sensitive and resistant species, at an MIC of 9.375 µg/mL (Figure 9). The output data were analyzed using a one-way ANOVA test

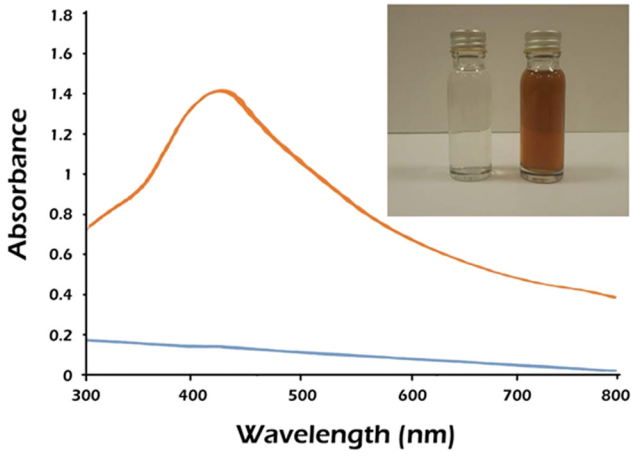

Figure 4: UV–vis spectra of silver nanoparticles synthesized using *A. solium* CFF of *A. solium* (orange curve), and the control group is represented herein by the (blue curve).

that did not show a degree of significance among all bacterial strains in sensitivity to the synthesized AgNPs (Figure 10).

4 Discussion

4.1 Fungal isolation and identification

The results of the morphological features of *A. solium* resembled that was shown by Hodhod et al. [31], in which the conidia are characterized by their large size along with an apical appendage. However, this study showed Pycnidia 330–380 µm high, 210–245 µm in diameter, and Conidia 37.5–46 × 13–18 µm, which is slightly different from the previous study, which showed Pycnidia 320–400 µm high and Conidia with 35–50 × 12.5–20 µm

Table 3: Trials and results of three factorial combinations of pH, temperature, and metal concentration

Experiment	pH	Temperature	Concentration	*R*1 Result/OD	*R*1 µg/mL	*R*2 Result/OD	*R*2 µg/mL	*R*3 Result/OD	*R*3 µg/mL
1	3	20	0.5	0.387	115.772	0.382	115.767	0.281	115.666
2	3	20	1	0.629	116.014	0.587	115.972	0.676	116.061
3	3	20	1.5	0.763	116.148	0.737	116.122	0.689	116.074
4	3	30	0.5	0.349	115.734	0.316	115.701	0.377	115.762
5	3	30	1	0.673	116.058	0.665	116.050	0.682	116.067
6	3	30	1.5	0.743	116.128	0.779	116.164	0.728	116.113
7	3	40	0.5	0.149	115.534	0.127	115.512	0.136	115.521
8	3	40	1	0.301	115.686	0.315	115.700	0.294	115.679
9	3	40	1.5	0.446	115.831	0.459	115.844	0.468	115.853
10	7	20	0.5	1.057	116.442	1.076	116.461	1.014	116.399
11	7	20	1	2.181	117.566	2.165	117.550	2.144	117.529
12	7	20	1.5	2.627	118.012	2.553	117.938	2.725	118.110
13	7	30	0.5	1.280	116.665	1.226	116.611	1.245	116.630
14	7	30	1	2.401	117.786	2.443	117.828	2.386	117.771
15	7	30	1.5	3.221	118.606	3.320	118.705	3.198	118.583
16	7	40	0.5	0.999	116.384	1.084	116.469	1.106	116.491
17	7	40	1	2.077	117.462	2.093	117.478	2.062	117.447
18	7	40	1.5	2.501	117.886	2.488	117.873	2.479	117.864
19	9	20	0.5	0.967	116.352	1.018	116.403	1.003	116.388
20	9	20	1	2.079	117.464	2.138	117.523	2.009	117.394
21	9	20	1.5	2.438	117.823	2.276	117.661	2.507	117.892
22	9	30	0.5	1.262	116.647	1.280	116.665	1.273	116.658
23	9	30	1	2.391	117.776	2.376	117.761	2.401	117.786
24	9	30	1.5	2.731	118.116	2.697	118.082	2.743	118.128
25	9	40	0.5	0.884	116.269	0.876	116.261	0.891	116.276
26	9	40	1	1.912	117.297	2.003	117.388	1.936	117.321
27	9	40	1.5	2.239	117.624	2.198	117.583	2.222	117.607

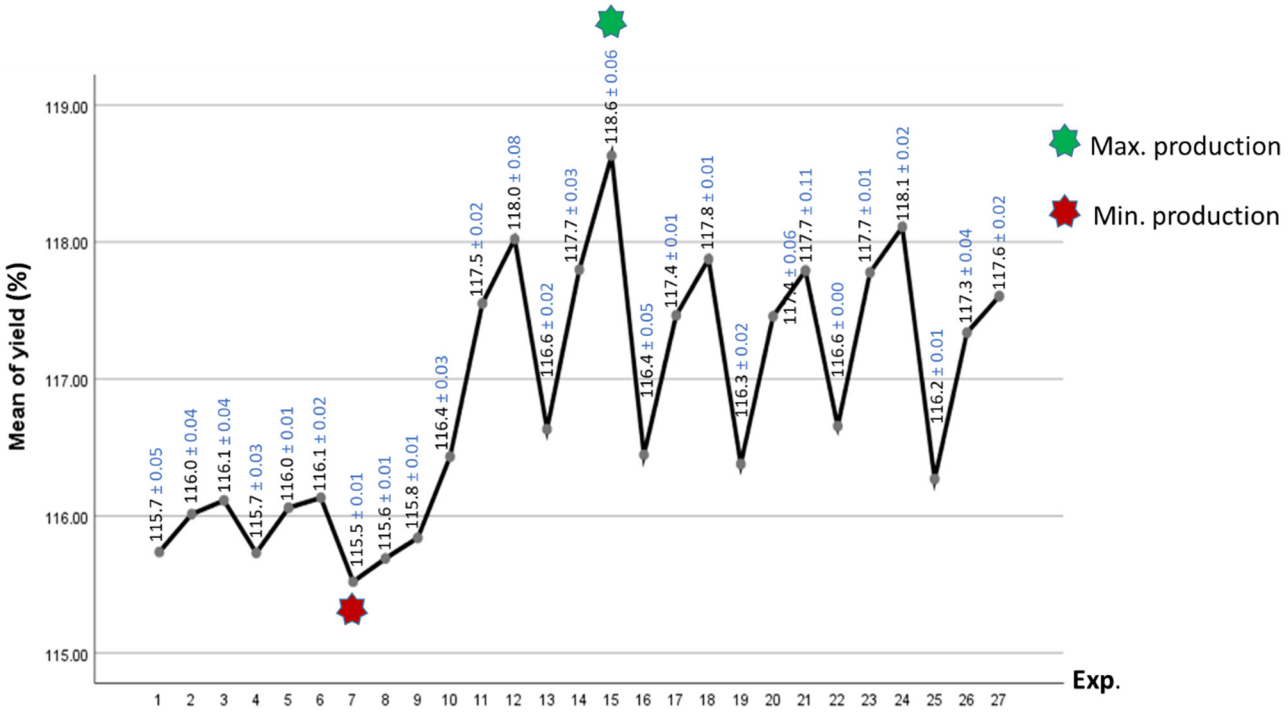

Figure 5: Means ± standard deviation of the yield (mg/mL) of AgNP produced from 27 experiments designed from all expected possibilities for temperature, metal salt concentration (mM), and pH. The green and red stars indicate the maximum and minimum significant production, respectively ($P < 0.05$).

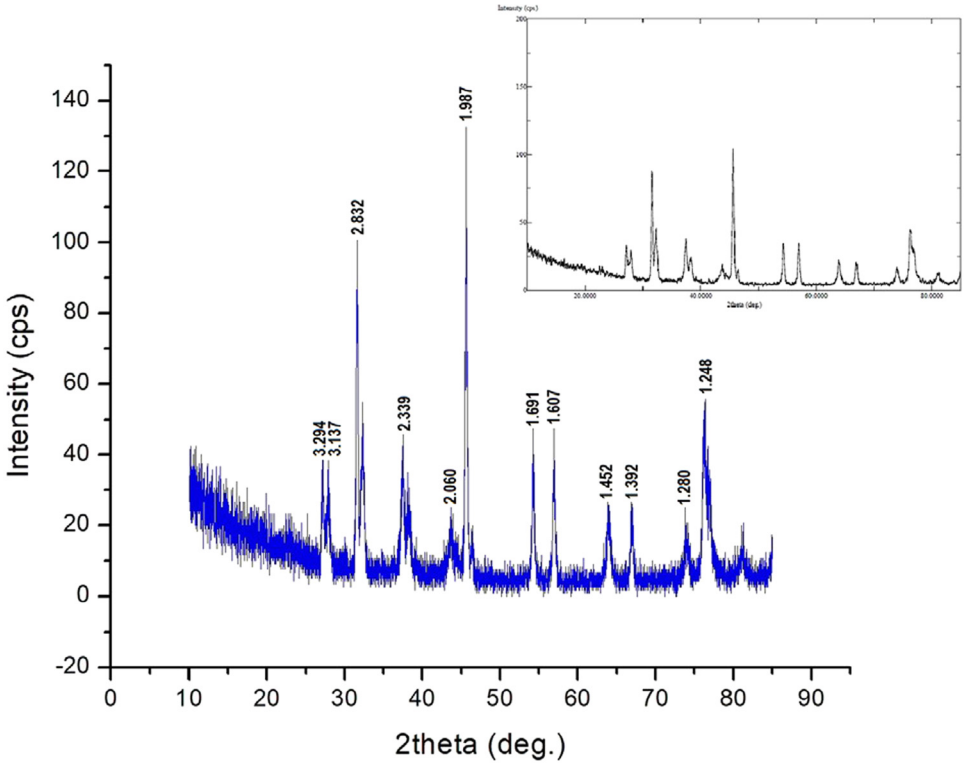

Figure 6: XRD pattern of silver nanoparticles synthesized by *A. solium*.

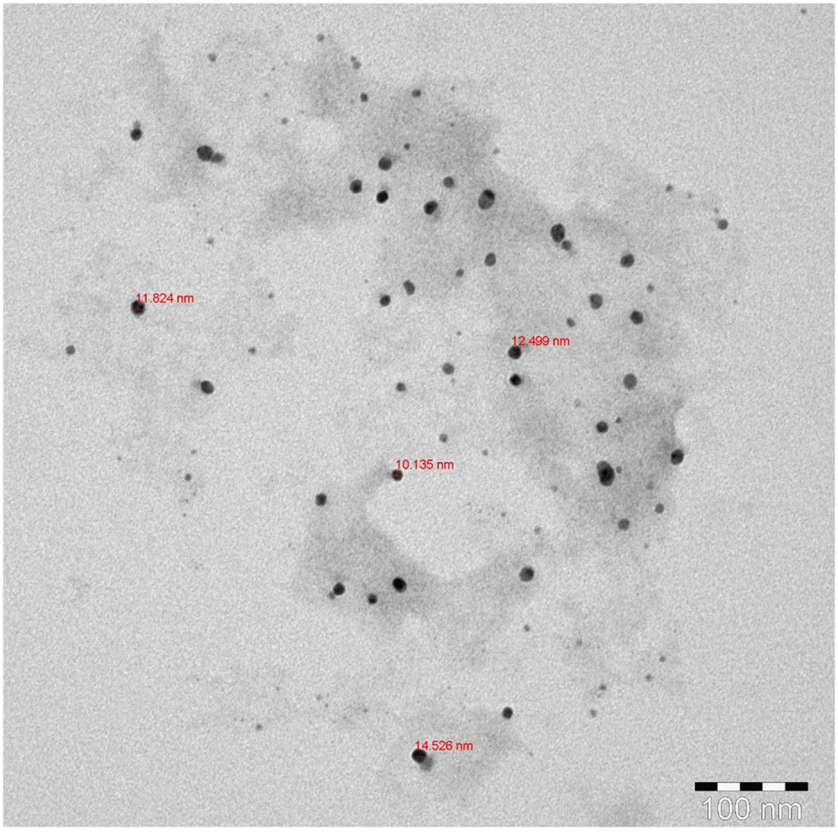

Figure 7: TEM micrograph of silver nanoparticles demonstrating shape and particle size estimation, where silver has a spherical form with an average mean size of 12 nm.

(Hodhod et al. [31]). Phylogenetic analysis placed the isolated fungus as a member of the Pleosporales Incertae-sedis family and formed a sister taxon of *A. solium* Abdel-Wahab, Hodhod, Bahkali, and K.D. Hyde. Forming a well-supported clade in both LSU and SSU data sets (100/100 for ML/MP, respectively).

4.2 AgNP synthesis

A. solium has been tested for its ability to biosynthesize AgNPs through an extracellular synthesis pathway, which depends on fungal secretions of bioactive molecules and enzymes in surrounding media [32–36]. Visual observation of silver metal bioreduction was observed due to color exchange from opaque to dark brown, as a result of excitation of free electrons in nanoparticles (Mohd Yusof et al., 2020). The emergence of a significant peak at 425 nm via UV–vis spectroscopy reveals the presence of a surface plasmon resonance, demonstrating that the silver metal was reduced to less than 100 nm. The shift in absorbance value suggests that the nanoparticles created are of various forms and/or sizes [37]. The heat treatment trials of the extracellular broth showed no sign of nanoparticle production in contrast to normal conditions because of the inhibition of bioactive extracellular compounds responsible for the biosynthesis of nanoparticles.

4.3 Factors affecting AgNP production

Optimization reactions applied during this study work aimed to support better growth of fungi, as well as enhance better yields of different m-NP, in which the best conditions will be further recommended for small-scale production. The factorial experiment design included three factors (temperature, metal salt concentration [mM], and pH) with three levels for each factor was carried out not only to study each factor as an individual parameter but also to observe the interaction between various factors combinations that will give the highest yield. Nanoparticle synthesis and the absorbance were applied as response variables [28].

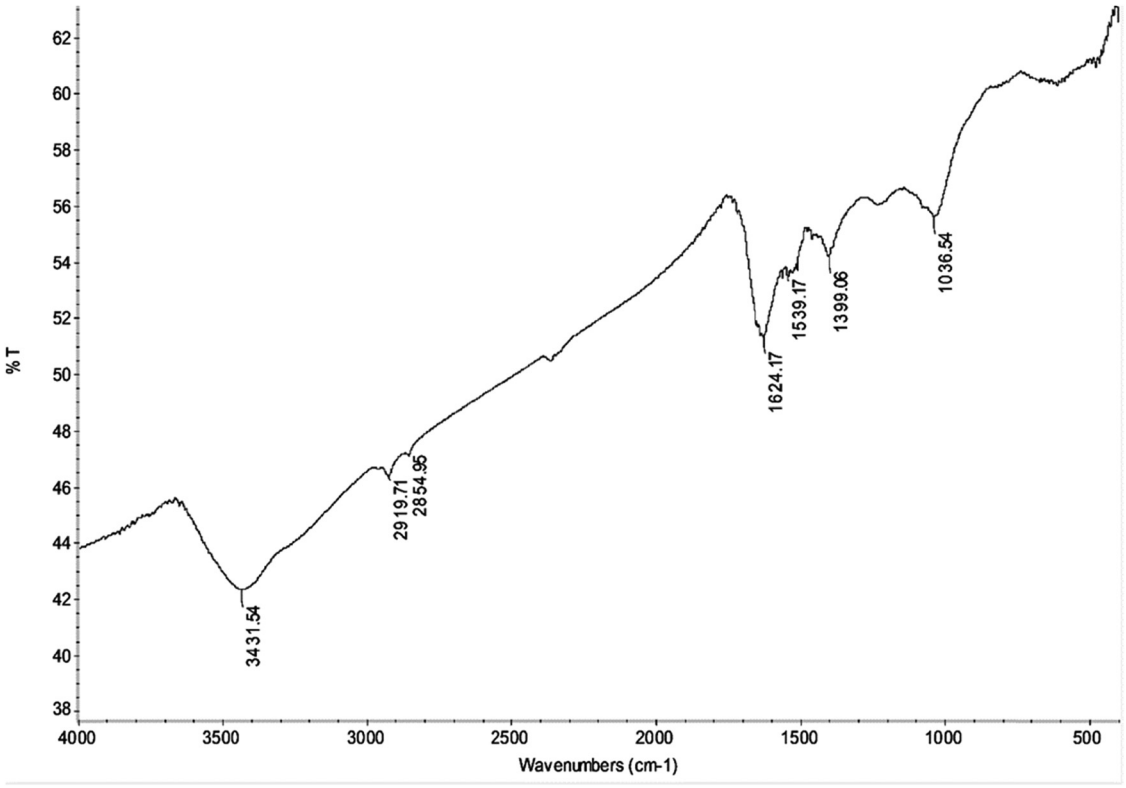

Figure 8: FTIR spectrum of the synthesized silver nanoparticles.

4.4 Effect of temperature

The results of temperature optimization revealed that it plays a key role in metal reduction, where the optimal temperature was 30°C with the maximum synthesis of AgNP, which remained stable for a longer period of time indicated a stabilized synthesis. The optimization reaction witnessed that manglicolous fungi favor medium heat temperatures of 30°C, which reflects the temperature of their original habitats, as marine environment from which it has

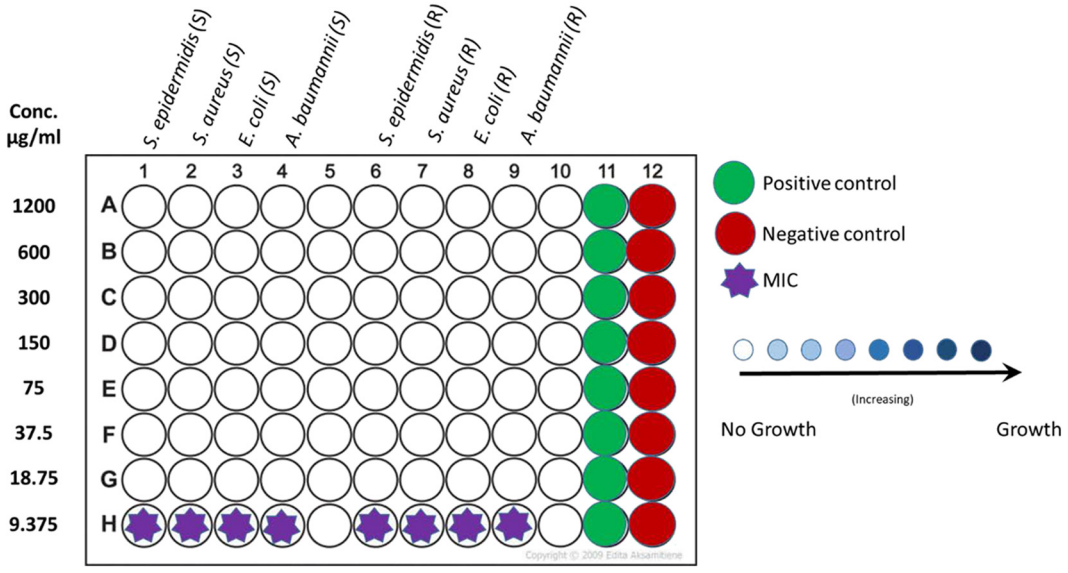

Figure 9: Microplate dilution was used to determine the MIC of the synthesized silver nanoparticles.

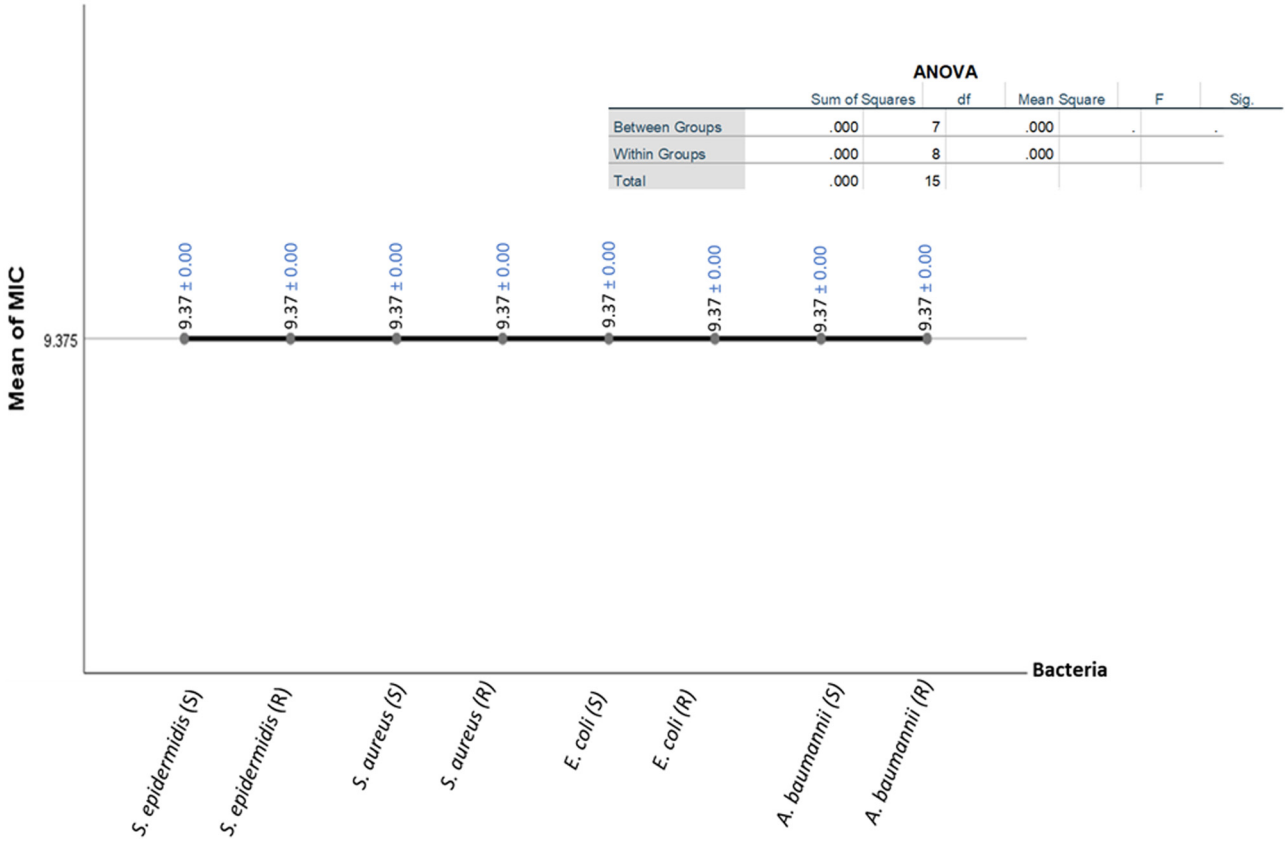

Figure 10: Mean plot of one-way MIC analysis of the synthesized silver nanoparticles.

been isolated the water temperature at the intertidal zone ranges from 25°C at night till 35°C in a day [38]. Unlike its terrestrial counterparts, which favor high temperatures, which can reach 80°C, as high degrees increase its kinetic energy and lead to a faster synthesis rate of metal biosynthesis rate for these species [39].

In general, the temperature of the reaction plays an important role in the characteristics and yield (%) of nanoparticles [40] and, furthermore, Lee et al. [41] reported that there is a significant association between the temperature and the time required for nanoparticle biosynthesis. The present findings correspond exactly to those reported in previous works on the role of temperature in the biosynthesis of nanoparticles.

4.5 Effect of metal salt concentration (mM)

The results of this study perfectly with several other studies which have shown that nanoparticles biosynthesis rate of nanoparticles increases with the metal salt concentration. Examples of these studies include the use of *Penicillium* sp. in AgNP biosynthesis, the maximum production rate was reached when the concentration of metal salt concentration was elevated from 0.2 to 2 mM [42]. *Sclerotinia sclerotiorum*, a plant pathogenic fungus, also registered the highest yield in an optimization reaction study for AgNP synthesis, when yield production increased along with metal concentration [29]. AgNPs produced by *F. oxysporum* in another study have also shown that its production rates increased with the addition of different concentrations of metal salts, starting from 1 up to 10 mM [43]. All of the above studies along with the current one revealed that metal salt concentration plays a key role in m-NP synthesis. The rate of bioreduction is directly proportional to the substrate concentration, as the reaction kinetics and morphology of the produced nanoparticle were directly affected by the concentration of the precursor solution (i.e., $AgNO_3$) [44–46].

4.6 Effect of pH

The results of the experiment help indicate that marine and coastal waters have relatively stable pH value within a small range from 7.6 to 8.3 (i.e., alkaline). Therefore, manglicolous fungi were in favor of pH levels giving higher

yield within alkaline media [47]. The study showed that pH is one of the key factors in the synthesis of different nanoparticles, since color formation was rapid at alkaline pH (7 and 9) compared to acidic pH [3]. Many studies confirmed the same result, including the optimization work made by [48]. Their work focused on the use of *F. oxysporum* in the biosynthesis of AgNPs; the results of this research showed that alkaline medium is more suitable for the synthesis of silver nitrate than low acidic pH, since the reduction rate of silver ions was higher at pH 8. Other fungal species showed the same results including *P. aeruginosa*, *S. sclerotiorum*, and *Trichoderma viride*; the results of all these studies revealed that alkaline pH is an essential factor that affects AgNP production, as high pH favors complete reduction of Ag+ into AgNP by providing electrons [29,49].

4.7 Optimization of AgNP synthesis

Optimization work was carried out to support better fungal growth and to improve the yield of different m-NP. Metal biosynthesis conditions, including metal concentration, pH, and temperature, were optimized throughout multiple trials. Maximum yield production was reached at conditions of (pH = 7, temperature = 30°C, and metal salt concentration [mM] = 1.5). The optimization work results correlate with many studies in regard to metal salts, as maximum production was obtained for AgNPs synthesized by *A. solium* with an increasing metal concentration. The same results were observed with *S. sclerotiorum* MTCC 8785, which was subjected to different concentrations of silver metal salts starting from 0.2 to 2 mM, the results of this study provided evidence that the increase in concentration up to 2 mM resulted in a complete reduction [29]. Similar observations have been reported with the results of Singh et al. [42] results, which showed maximum AgNP synthesis at 2 mM $AgNO_3$ concentration using *Penicillium* species. The pH conditions showed similar observations during the optimization process, as *A. solium* favored medium to basic pH (7 and 9) for stable metal bioreduction, which is correlated with other reported studies, including that in the case of *P. aeruginosa* [50] and *T. viride* [49], the results of both studies revealed that stable m-NP and their complete reduction occur in medium to basic medium, in which electrons are provided to mediate the reaction. However, the temperature conditions showed irrelevant results, since maximum production was obtained at a medium temperature of (30°C). Many studies have reported maximum biosynthesis at elevated temperatures, such as that conducted by Saxena et al. [29] who evaluated the effect of temperature on AgNP production by *S. sclerotiorum*, as reactions were incubated at different temperatures from 20 to 80°C with a difference of 20°C and then monitored for AgNPs synthesis. The results of that study observed the maximum synthesis of AgNP at 80°C, which remained stable for a long period. In another case study, high temperature was found to impart increased kinetic energy and lead to a faster synthesis rate [39]. The results of the current study showed stable and maximum production at normal temperature, thus an advantageous condition resulting in cost-effective production. The minimum production of yield was observed under the conditions (pH = 3, temperature = 40°C and metal salt concentration [mM] = 0.5). These results resemble those observed by many studies [29,39,49].

Optimization outcome results recommend the utilization of manglicolous fungi for nanoparticles production because of many advantageous characteristics and potentials possessed by this fascinating group of fungi, including ease in maintaining, control, and containment. *A. solium* showed a fast-growing and producing nanofactory, which reflects its ability to accumulate massive amounts of metals. Furthermore, the medium was easily filtered to obtain cell-free filtration (CFF), making the entire process very easy; this will be more cost-effective on the industrial scale [9].

4.8 Characterization of AgNPs

XRD of AgNPs peaks reflected on the characteristic FCC silver lines indexed as (2.832), (1.987), (1.280), and (1.248) that were observed in these samples at diffraction angles of 32.6°, 46.1°, 74.7°, and 77.6°, respectively. The AgNPs calculated by XRD data had a mean size of 20 nm. The acquired AgNP data fitted the database of Joint Committee on Powder Diffraction Standards (JCPDS) file No. 04-0783 completely [51]. The TEM data revealed only a spherical shape with an average size of 12 nm, indicating that *A. solium* has silver reduction potentials. Both XRD and TEM data agreed exactly, validating the features and properties [52,53].

The apparent existence of proteins surrounding and encapsulating produced AgNPs was verified by FTIR analysis, which acts as a reducing and stabilizing agent throughout the biosynthesis process [29,54]. The findings of the AgNP characterization were consistent with those of other research. The absorbance of AgNPs was detected at 380, 400, 413, 425, and 430 nm, which was within the range of previously reported data [29,55–57]. The variation in absorbance value suggests that the generated nanoparticles are of various forms and/or sizes [37].

The XRD results of the AgNP data obtained were perfectly matched with the database of JCPDS file No. 04-0783 [51]; this was further documented in other studies at kind

of different angles (Mechouche [55,58]). The TEM results for AgNP from *A. solium* appeared with only spherical shape and an average size of 12 nm, which was not comparable to many studies related to fungi due to its small size but more similar to nanoparticles synthesized by plants, such as those observed in *Lantana camara*, which reduced the silver metal salt to 14 nm [56]. FTIR examination verified the existence of proteins surrounding and coating the produced AgNPs, which is consistent with the findings of much other research [54,55].

4.9 Antibacterial activity

In the current study, AgNPs synthesized by *A. solium* showed very promising wide-range activity results, reflecting its great potentials, and high antibacterial activity was shown against all Gram-positive and -negative bacteria, including sensitive and resistant species at a concentration of 9.375 µg/mL. The results demonstrated that the produced m-NP played a critical role in inflicting significant damage to bacterial cells, with the tiny AgNPs (i.e., 12 nm) demonstrating superior antibacterial activity. The increased surface area of Ag+ small particles resulted in better surface contact with bacteria and, thus, a higher bactericidal action [35,59,60].

Ag^{+} ions are thought to form an electrical interaction with the bacterial outer surface, and upon contact, the bacterial cells are quickly oxidized and destroyed. This occurs given that AgNPs unleash their ions, which react directly with the thiol (–SH) group of proteins in the bacterial cell and protrude across the cell membrane. As a result, inhibiting membrane permeability causes bacterial cell death [61].

Finally, the results of this study recommend the application of AgNPs synthesized by *A. solium* in the pharmaceutical industry. Furthermore, the demonstration of the produced nanoparticles against other pathogenic bacteria alone or with antibiotics [62], to observe any other activities.

5 Conclusion

The cost-effective green synthesis of stable AgNPs through the utilization of marine fungi as a new biological resource showed great potential during the current study. Culture extract of *A. solium* used herein as a reducing agent in the nanoparticle synthesis process; optimization work to obtain better fungal growth revealed its effectiveness; thus, it could be scaled up for commercial production on an industrial level due to promising criteria that showed of time savings, low cost, and also a nonhazardous effect on the environment. The characterization of the size and shape was carried out via XRD and TEM, which proved to be valuable tools to demonstrate the small-sized 12 nm, which possesses a spherical shape structure. FTIR analysis revealed that the proteins surrounding the synthesized AgNPs play a crucial role in stabilizing them during the biosynthesis process. The nanoparticles produced were confirmed to have promising antibacterial activity and hence could be implemented in various biomedical approaches. Finally, other locations and other substrates should be investigated for marine fungi to be utilized in different biotechnological applications.

Acknowledgements: The authors extend their appreciation to the Researchers Supporting Project number RSPD2024R686, King Saud University, Riyadh, Saudi Arabia.

Funding information: The research was financially supported by Researchers Supporting Project number RSPD2024R686, King Saud University, Riyadh, Saudi Arabia.

Author contributions: All authors contributed to the preparation of the manuscript and discussion.

Conflict of interest: On behalf of all authors, the corresponding author states that there is no conflict of interest.

Ethical approval: The conducted research is not related to either human or animal use.

Data availability statement: Derived data supporting the findings of this study are available from the corresponding author on request.

References

[1] Basak S, Singh P, Rajurkar M. Multidrug resistant and extensively drug resistant bacteria: a study. J Pathog. 2016;2016:4065603.
[2] Hall W, McDonnell A, O'Neill J. Superbugs: An arms race against bacteria. Cambridge, Massachusetts, United States: Harvard University Press; 2018.
[3] van den Brink R. The end of an antibiotic era. New York, NY, USA: Springer; 2021 p. 15–45.
[4] Wang L, Hu C, Shao L. The antimicrobial activity of nanoparticles: present situation and prospects for the future. Int J Nanomed. 2017;12:1227–49.
[5] Nachiyar V, Sunkar S, Prakash P. Biological synthesis of gold nanoparticles using endophytic fungi. Der Pharma Chem. 2015;7(11):31–8.
[6] Ottoni CA, Simões MF, Fernandes S, Dos Santos JG, Da Silva ES, de Souza RFB, et al. Screening of filamentous fungi for antimicrobial silver nanoparticles synthesis. AMB Express. 2017;7(1):31.

[7] Shende S, Ingle AP, Gade A, Rai M. Green synthesis of copper nanoparticles by Citrus medica Linn.(Idilimbu) juice and its antimicrobial activity. World J Microbiol Biotechnol. 2015;31(6):865–73.
[8] Mandal D, Bolander ME, Mukhopadhyay D, Sarkar G, Mukherjee P. The use of microorganisms for the formation of metal nanoparticles and their application. Appl microbiol Biotechnol. 2006;69(5):485–92.
[9] Rahimi G, Alizadeh F, Khodavandi A. Mycosynthesis of silver nanoparticles from Candida albicans and its antibacterial activity against Escherichia coli and Staphylococcus aureus. Trop J Pharm Res. 2016;15(2):371–5.
[10] Lekha DC, Shanmugam R, Madhuri K, Dwarampudi LP, Bhaskaran M, Kongara D, et al. Review on silver nanoparticle synthesis method, antibacterial activity, drug delivery vehicles, and toxicity pathways: recent advances and future aspects. J Nanomater. 2021;2021:1–11.
[11] Devika R, Elumalai S, Manikandan E, Eswaramoorthy D. Biosynthesis of silver nanoparticles using the fungus Pleurotus ostreatus and their antibacterial activity. Open Access Sci Rep. 2012;1:557.
[12] Akter S, Huq MA. Biologically rapid synthesis of silver nanoparticles by Sphingobium sp. MAH-11T and their antibacterial activity and mechanisms investigation against drug-resistant pathogenic microbes. Artif Cells Nanomed Biotechnol. 2020;48(1):672–82.
[13] Hamouda RA, Hussein MH, Abo-Elmagd RA, Bawazir SS. Synthesis and biological characterization of silver nanoparticles derived from the cyanobacterium Oscillatoria limnetica. Sci Rep. 2019;9(1):13071.
[14] Huq MA. Green synthesis of silver nanoparticles using Pseudoduganella eburnea MAHUQ-39 and their antimicrobial mechanisms investigation against drug resistant human pathogens. Int J Mol Sci. 2020;21(4):1510.
[15] Rafique M, Sadaf I, Rafique MS, Tahir MB. A review on green synthesis of silver nanoparticles and their applications. Artif Cells Nanomed Biotechnol. 2017;45(7):1272–91.
[16] Salem SS, Fouda A. Green synthesis of metallic nanoparticles and their prospective biotechnological applications: an overview. Biol Trace Elem Res. 2021;199:344–70.
[17] Jones EG. Marine fungi: some factors influencing biodiversity. Fungal Diversity. 2000;4(193):53–73.
[18] Thatoi H, Behera BC, Mishra RR, Dutta SK. Biodiversity and biotechnological potential of microorganisms from mangrove ecosystems: a review. Ann Microbiol. 2013;63(1):1–19.
[19] Jones EG, Suetrong S, Sakayaroj J, Bahkali AH, Abdel-Wahab MA, Boekhout T, et al. Classification of marine ascomycota, basidiomycota, blastocladiomycota and chytridiomycota. Fungal Diversity. 2015;73(1):1–72.
[20] Abdel-Wahab MA, Bahkali AH, Jones EG, Elgorban AM, Abdel-Aziz FA, Hodhod MS, et al. Two new species of Kallichroma (Bionectriaceae, Hypocreales) from Saudi Arabian mangroves. Phytotaxa. 2016;260(1):66–74.
[21] Vilgalys R, Hester M. Rapid genetic identification and mapping of enzymatically amplified ribosomal DNA from several Cryptococcus species. J Bacteriol. 1990;172(8):4238–46.
[22] White T. Analysis of phylogenetic relationships by amplification and direct sequencing of ribosomal genes. PCR Protocols: A Guide Methods Appl. 1990;315–22.
[23] Thompson JD, Gibson TJ, Plewniak F, Jeanmougin F, Higgins DG. The CLUSTAL_X windows interface: flexible strategies for multiple sequence alignment aided by quality analysis tools. Nucleic Acids Res. 1997;25(24):4876–82.
[24] Kumar S, Stecher G, Li M, Knyaz C, Tamura K. MEGA X: molecular evolutionary genetics analysis across computing platforms. Mol Biol Evol. 2018;35(6):1547.
[25] Felsenstein J. Confidence limits on phylogenies: an approach using the bootstrap. Evolution. 1985;39(4):783–91.
[26] Tamura K, Nei M. Estimation of the number of nucleotide substitutions in the control region of mitochondrial DNA in humans and chimpanzees. Mol Biol Evolution. 1993;10(3):512–26.
[27] Das VL, Thomas R, Varghese RT, Soniya E, Mathew J, Radhakrishnan E. Extracellular synthesis of silver nanoparticles by the Bacillus strain CS 11 isolated from industrialized area. 3 Biotech. 2014;4(2):121–6.
[28] Saha N, Gupta SD. Biogenic synthesis and structural characterization of polyshaped gold nanoparticles using leaf extract of Swertia chirata along with process optimization by response surface methodology (RSM). J Clust Sci. 2016;27(4):1419–37.
[29] Saxena J, Sharma PK, Sharma MM, Singh A. Process optimization for green synthesis of silver nanoparticles by Sclerotinia sclerotiorum MTCC 8785 and evaluation of its antibacterial properties. SpringerPlus. 2016;5(1):861.
[30] Cullity BD. Elements of X-ray diffraction. Addison. Wesley Mass; 1978.
[31] Hodhod MS, Abdel-Wahab MA, Bahkali AH, Hyde KD. Amarenographium solium sp. nov. from Yanbu mangroves in the Kingdom of Saudi Arabia. Cryptogam Mycol. 2012;33(3):285–94.
[32] Durán N, Marcato PD, Durán M, Yadav A, Gade A, Rai M. Mechanistic aspects in the biogenic synthesis of extracellular metal nanoparticles by peptides, bacteria, fungi, and plants. Appl Microbiol Biotechnol. 2011;90(5):1609–24.
[33] Li X, Xu H, Chen Z-S, Chen G. Biosynthesis of nanoparticles by microorganisms and their applications. J Nanomater. 2011;2011:270974.
[34] Mohanpuria P, Rana NK, Yadav SK. Biosynthesis of nanoparticles: technological concepts and future applications. J Nanopart Res. 2008;10(3):507–17.
[35] Prabhu S, Poulose EK. Silver nanoparticles: mechanism of antimicrobial action, synthesis, medical applications, and toxicity effects. Int Nano Lett. 2012;2(1):32.
[36] Sathiyanarayanan G, Dineshkumar K, Yang Y-H. Microbial exopolysaccharide-mediated synthesis and stabilization of metal nanoparticles. Crit Rev Microbiology. 2017;43(6):731–52.
[37] Desai R, Mankad V, Gupta SK, Jha PK. Size distribution of silver nanoparticles: UV-visible spectroscopic assessment. Nanosci Nanotechnol Lett. 2012;4(1):30–4.
[38] El-Sharouny H, Raheem A, Abdel-Wahab M. Manglicolous fungi of the red sea in upper Egypt. Microbiol Res. 1998;153(1):81–96.
[39] Birla SS, Gaikwad SC, Gade AK, Rai MK. Rapid synthesis of silver nanoparticles from *Fusarium oxysporum* by optimizing physicocultural conditions. Sci World J. 2013;2013:796018.
[40] Jiang X, Chen W, Chen C, Xiong S, Yu A. Role of temperature in the growth of silver nanoparticles through a synergetic reduction approach. Nanoscale Res Lett. 2011;6(1):32.
[41] Lee S-W, Chang S-H, Lai Y-S, Lin C-C, Tsai C-M, Lee Y-C, et al. Effect of temperature on the growth of silver nanoparticles using plasmon-mediated method under the irradiation of green LEDs. Materials. 2014;7(12):7781–98.
[42] Singh P, Kim Y-J, Zhang D, Yang D-C. Biological synthesis of nanoparticles from plants and microorganisms. Trends Biotechnol. 2016;34(7):588–99.

[43] Korbekandi H, Ashari Z, Iravani S, Abbasi S. Optimization of biological synthesis of silver nanoparticles using Fusarium oxysporum. Iran J Pharm Res: IJPR. 2013;12(3):289.
[44] Christensen L, Vivekanandhan S, Misra M, Mohanty AK. Biosynthesis of silver nanoparticles using murraya koenigii (curry leaf): an investigation on the effect of broth concentration in reduction mechanism and particle size. Adv Mater Lett. 2011;2(6):429–34.
[45] Khan M, Khan M, Adil SF, Tahir MN, Tremel W, Alkhathlan HZ, et al. Green synthesis of silver nanoparticles mediated by Pulicaria glutinosa extract. Int J Nanomed. 2013;8:1507.
[46] Singh AK, Talat M, Singh D, Srivastava O. Biosynthesis of gold and silver nanoparticles by natural precursor clove and their functionalization with amine group. J Nanopart Res. 2010;12(5):1667–75.
[47] Brotowidjoyo MD, Tribawono D, Mulbyantoro E. Introduction to water environmental and aquaculture. Yogyakarta, Indonesia: Publisher Liberty; 1995.
[48] Khan N, Jamme J. Optimization of reaction parameters for silver nanoparticles synthesis from Fusarium Oxysporum and determination of silver nanoparticles concentration. J Mater Sci Eng. 2016;5(283):2169-0022.1000283.
[49] Chitra K, Annadurai G. Bioengineered silver nanobowls using Trichoderma viride and its antibacterial activity against gram-positive and gram-negative bacteria. J Nanostruct Chem. 2013;3(1):9.
[50] Mohammadinia M, Rahmani S, Eslami G, Ghassemi-Broumand M, Amiri MA, Aghaie G, et al. Contact lens disinfecting solutions antibacterial efficacy: comparison between clinical isolates and the standard ISO ATCC strains of Pseudomonas aeruginosa and Staphylococcus aureus. Eye. 2012;26(2):327.
[51] Krishnaraj C, Ramachandran R, Mohan K, Kalaichelvan P. Optimization for rapid synthesis of silver nanoparticles and its effect on phytopathogenic fungi. Spectrochim Acta Part A: Mol Biomol Spectrosc. 2012;93:95–9.
[52] Chicea D, Indrea E, Cretu C. Assesing Fe3O4 nanoparticle size by DLS, XRD and AFM. J Optoelectron Adv Mater. 2012;14(5):460.
[53] Hu C, Zhang Z, Liu H, Gao P, Wang ZL. Direct synthesis and structure characterization of ultrafine CeO2 nanoparticles. Nanotechnology. 2006;17(24):5983.
[54] Daima HK, Selvakannan P, Shukla R, Bhargava SK, Bansal V. Fine-tuning the antimicrobial profile of biocompatible gold nanoparticles by sequential surface functionalization using polyoxometalates and lysine. PLoS one. 2013;8(10):e79676.
[55] Abdel-Hadi AM, Awad MF, Abo-Dahab NF, ElKady MF. Extracellular synthesis of silver nanoparticles by Aspergillus terreus: biosynthesis, characterization and biological activity. Biosci Biotechnol Res Asia. 2014;11(3):1179–86.
[56] Ajitha B, Reddy YAK, Reddy PS. Green synthesis and characterization of silver nanoparticles using Lantana camara leaf extract. Mater Sci Eng: C. 2015;49:373–81.
[57] Aromal SA, Philip D. Green synthesis of gold nanoparticles using Trigonella foenum-graecum and its size-dependent catalytic activity. Spectrochim Acta Part A: Mol Biomol Spectrosc. 2012;97:1–5.
[58] Zayed MF, Eisa WH. Phoenix dactylifera L. leaf extract phytosynthesized gold nanoparticles; controlled synthesis and catalytic activity. Spectrochim Acta Part A: Mol Biomol Spectrosc. 2014;121:238–44.
[59] Cho K-H, Park J-E, Osaka T, Park S-G. The study of antimicrobial activity and preservative effects of nanosilver ingredient. Electrochim Acta. 2005;51(5):956–60.
[60] Panyala NR, Peña-Méndez EM, Havel J. Silver or silver nanoparticles: a hazardous threat to the environment and human health? J Appl Biomed. 2008;6(3):117–29.
[61] Zhang H, Chen G. Potent antibacterial activities of Ag/TiO2 nanocomposite powders synthesized by a one-pot sol−gel method. Environ Sci Technol. 2009;43(8):2905–10.
[62] Ganie MA, Khurana ML, Nisar S, Shah PA, Shah ZA, Kulshrestha B, et al. Improved efficacy of low-dose spironolactone and metformin combination than either drug alone in the management of women with polycystic ovary syndrome (PCOS): a six-month, open-label randomized study. J Clin Endocrinol Metab. 2013;98(9):3599–607.